



Hall current effect on unsteady rotational flow of carbon nanotubes with dust particles and nonlinear thermal radiation in Darcy–Forchheimer porous media

M. Bilal¹ · M. Ramzan²

Received: 31 October 2018 / Accepted: 27 April 2019 / Published online: 13 May 2019
© Akadémiai Kiadó, Budapest, Hungary 2019

Abstract

The present discussion is about the unsteady two-dimensional flow of mixed convection and nonlinear thermal radiation in the presence of water-based carbon nanotubes over the vertically convected stretched sheet embedded in a Darcy–Forchheimer porous media. Saffman’s proposed model is used for the suspension of fine dust particles in the nanofluid. A strong magnetic field (MHD) is applied normal to the flow which governs the Hall current effects. Khanafer Vafai Lightstone model estimated the effect of thermal conductivity and viscosity of the carbon nanotubes. Boundary layer approximation is utilized to built the nonlinear partial differential equations (PDEs). Similarity transformation is applied to convert these PDEs into the system of ordinary differential equations. Problem is solved numerically by *bvp4c*, using MATLAB software. It is observed through the analysis that the thermal field of nanofluid and the temperature boundary layer are much more higher than that of the dust phase, and these are further enhanced for the higher radiation parameter.

Keywords Hall current · Nonlinear thermal radiation · Dusty carbon nanotubes · Mixed convection · Darcy–Forchheimer media

List of symbols

b, α	A real constant	K^*	Permeability of porous medium
B_0	Magnetic induction ($\text{kg s}^{-2} \text{A}^{-1}$)	l	Mass concentration of dust
Bi	Biot number	m_p	Mass of dust particles
C	Specific heat ($\text{J kg}^{-1} \text{K}^{-1}$)	Nu	Local Nusselt number
E	Intensity vector of the electric field	n_e	Number density of electron
F'	Dimensionless velocity of dust	P_e	Electron pressure
F	Inertia coefficient of porous medium	P	Pressure
F_p	Force due to dust particles	Pr	Prandtl number
F_b	Body forces	Q_p	Thermal interaction between nanoparticles and dust phase
f'	Dimensionless velocity	q_w	Surface heat flux
F_r	Inertia coefficient	q_r	Radiation heat flux
g	Gravitational acceleration (m s^{-2})	Rd	Thermal radiation parameter
Gr_x	Grashof number	r_p	Radius of dust particles
h	Dimensionless transverse velocity	Re_x	Local Reynolds number
h_c	Heat flux coefficient ($\text{W m}^{-1} \text{K}^{-1}$)	S	Unsteadiness parameter
J	Current density vector	t	Time
		t	Fluid temperature (K)
		U_w	Deformation velocity of the sheet
		$U(u, v, w)$	Velocity vector (m s^{-1})
		$V(u, v, w)$	Velocity vector (m s^{-1})
		(x, y, z)	Axial and normal coordinates
		β_v	Momentum dust parameter

✉ M. Bilal
m.bilal@math.uol.edu.pk

¹ Department of Mathematics, University of Lahore, Chenab Campus, Gujrat, Pakistan

² Bahria University, Islamabad, Pakistan

β_T	Thermal expansion coefficient
β_t	Thermal dust parameter
γ	Specific heat ratio
δ	Porosity parameter
η	Dimensionless normal distance
θ	Dimensionless temperature
θ_w	Temperature ratio parameter
κ	Thermal conductivity ($\text{W m}^{-1} \text{K}^{-1}$)
λ	Mixed convection parameter
μ	Dynamic viscosity
σ	Electric conductivity
σ^*	Stefan–Boltzmann constant ($\text{m}^2 \text{s}^{-1}$)
τ_e	Electron collision time
τ_T	Thermal relaxation time of dust phase
τ_v	Momentum relaxation time of dust phase
τ_{wx}	Wall shear stress in x direction
ω	Frequency
ω_e	Electron frequency
\varkappa	Nanoparticle volume fraction
ψ	Stream function ($\text{m}^2 \text{s}^{-1}$)
Ω	Rotational parameter
\sphericalangle	Absorption coefficient

Subscripts

nf	Nanofluid
f	Base fluid
s	Nanoparticles (CNTs)
p	Dust phase/particles
w	Wall
e	Charge on electron

Introduction

The existence of very small-sized (micro or millimeter) particles or impurities in the fluid is quite natural. Such fluids are called the dusty fluids. Due to these dust particles, the thermal property of such fluids is increased [1]. The suspension of dust particles in the base fluid can degrade its efficiency in the devices or machines, but still it is beneficial in respect of fluid flow and increment in thermal conductivity. There are several scientific and engineering processes where the involvement of dusty particles plays an important role such as slurries movements in chemical and nuclear processes, lunar ash flows and powder technology, oceanography, medicine, blood flow in arteries, steel manufacturing industry, waste water treatment, dust in gas cooling systems and corrosive particles in engine oil flow. Initially, Farbar and Morley [2] analyzed experimentally about the transport of heat for the gas-solid suspensions. Stability analysis and influences of dust particles in viscous and laminar flow were first time

studied by Saffman [3]. Hazem et al. [4] studied the combined effects of viscous dissipation, Hall current, Joule heating and ion slip effects on unsteady Couette flow of a dusty fluid which is electrically conducting and incompressible with strong magnetic field and injection suction phenomenon. They found that the dust velocities are highly influenced by Hall and ion-slip effects. Koneri et al. [5] have discussed numerically about the dusty upper-convected Maxwell fluid over the convectively heated sheet with nonlinear thermal radiation, viscous dissipation and magnetic field. Shooting method is opted to solve the problem. Unsteady dusty nanofluid flow over the permeable exponentially stretching sheet with strong magnetic field and radiation effects was covered by Sandeep et al. [6]. Copper and copper oxide are used with dust particles. They observed the increment in heat transfer rate when the fluid particle interaction is enhanced. Pop et al. [7] addressed the dusty fluid flow over the two-dimensional shrinking surface. Problem is formulated using boundary layer approximation and solved by `bvp4c`. Ghadikolaei et al. [8] investigated boundary layer dusty micropolar nanofluid flow and heat transfer with MHD and thermal radiation embedded in the porous medium. They considered the TiO_2 as a nanoparticles in water. Heat and fluid flow of Casson dusty fluid in the presence of nonlinear radiation over a vertical wavy cone is addressed numerically by Sadia et al. [9]. Gireesha et al. [10] considered the time-dependent flow of water-based copper nanofluid having dust particles with effective viscosity and thermal conductivity using additionally the Hall effects over the stretching sheet. It is witnessed that the heat transfer rate is increased due to the higher concentration of dust particles.

Henry Darcy, a French engineer, suggested the flow model of liquids or gases or their mixtures through a porous sand bed medium in 1856. It links the velocity of the fluid and the pressure drop during the flow. It can be stated in mathematical form as follows [11–13]:

$$-\frac{dp}{dx} = \frac{1}{k} \cdot (\mu \cdot v_f),$$

where v_f is the filtration velocity. This law works correctly for the low porosity and the fluid having smaller velocity. On the other hand, if the velocities are higher, then a discrepancy appears between the experimental data and the obtained results. Darcy's law can only be applicable when the range of Reynold's number is $1 \leq Re \leq 10$ [11, 14]. This flow in Darcy's law is linked with inertial impacts by Forchheimer [15] proposing the kinetic energy term [11, 12, 16].

$$-\frac{dp}{dx} = \frac{1}{k} \cdot (\mu \cdot v_f) + F \cdot (\rho + v_f^2),$$

where F is the non-Darcy coefficient also know an Forchheimer coefficient. Fluids having high flow rate in the porous medium have significant importance in engineering and industries like petroleum technology, hydrology, agriculture, mining and mineral processes, catalytic reactors, geophysics and many others [17]. Rami et al. [18] modeled mathematically the mixed convective non-Darcian flow through a vertical flat plate under mass and thermal diffusion effects embedded in a porous medium and found its similarity solutions. Sobieskil and Trykozko [19] conduct an experimental study based on the pressure drop and flow rate in which the Forchheimer and permeability coefficients are studied. They have correctly determined the ranges for Darcy's and Forchheimer's laws and determined their related issues. Hayat et al. [20] conducted a study on the Darcy–Forchheimer viscoelastic fluids flowing with Cattaneo-Christov heat flux and homogeneous heterogeneous reactions over the sheet. They have used two different types of viscoelastic fluids and compared their results. Darcy–Forchheimer flow of MHD Maxwell nanofluid over the convective sheet is discussed by Taseer et al. [21]. Brownian motion and thermophoresis effects along with zero mass flux condition is also considered. The work of Taseer et al. [21] is extended by Sajid et al. [22] in which the effects of nonlinear thermal radiation, variable thermal conductivity and activation energy are also incorporated. Three-dimensional convective flow of Darcy–Forchheimer porous medium over bidirectional stretching sheet in the presence of water-based single- and double-walled carbon nanotubes is discussed by Abdullah [23].

In recent era, the use of conventional fluids in industries for the heat transfer purpose is almost ceased, and these are replaced with nanofluid, comprising of pure liquid and nanosized particles [24–34]. The main purpose of the fluid flow is to analyze the heat and mass transfer over different geometries [35–38]. After numerous experiments, it is believed that different nanoparticles have different capacity to conduct heat. Shape and size of the nanoparticles are also matters [39]. Experiments yield about six times greater thermal conductivity of the nanofluid in the presence of carbon nanotubes (CNT) instead of other nanoparticles [40]. Carbon nanotubes are in cylindrical shape and are crystalline allotropes of carbon. Their uni-dimensional structure enhances their mechanical and electronic properties [41, 42]. Choi and his coworker [43] first time experimentally reported the enhanced thermal properties of base fluid in the presence of cylindrical carbon nanotubes. The applications of CNT can be seen in nanotechnology, I/R optics industries, semiconductor devices, ultra-

capacitors, atomic force microscope, radar-absorbing coating, etc. Single-walled and multiwalled CNT are two basic categories of carbon nanotubes. In the present article, we have focused the single-walled carbon nanotubes, because of their ability to form a network of carbon atoms with surrounding atoms and thereby responsible to increase the thermal conductivity.

The literature review reveals that there have been studies about the CNTs in varied geometries. However, fewer are reported in case of dust particles. The main purpose of this dissertation is to model and analyze the Darcy–Forchheimer time-dependent flow and heat transfer of water-based SWCNTs over the convective sheet and in the presence of nonlinear thermal radiation, heat generation/absorption and Hall current effects. Due to the impurities, the dust phase of nanofluid is also discussed in detail. To the best of our knowledge, no such study is conducted before in the literature. A mathematical model is solved numerically by `bvp4c`, a built-in MATLAB function. The Nusselt number and the skin friction coefficients are computed and discussed. Results are calculated and presented in tables and graphs. Finally, the prominent findings are highlighted.

Mathematical formulation

Time-dependent two-dimensional non-Darcian laminar, rotational and incompressible water-based CNT over the convectively stretching sheet is considered to flow along the x -axis. Strong magnetic field which is responsible to generate the Hall current effects is applied normal to the flow by ignoring the induced magnetic field. During the formulation of energy equation, the Khanafer Vafai Lightstone (KVL) model is used for the effective thermal conductivity and viscosity of the fluid, along with nonlinear thermal radiation and heat generation absorption effects. The presence of dust particles in the fluid is assumed to be uniform in size and conducting which are initially in rest. The number density of dust particles is consistance all through the stream. The mixture theory and phenomenological laws for the CNT are as follows [44]: Mixture theory

$$\rho_{nf} = (1 - \chi)\rho_f + \chi\rho_s, \quad (1)$$

$$(\rho\beta_T)_{nf} = (1 - \chi)(\rho\beta_T)_f + \chi(\rho\beta_T)_s, \quad (2)$$

$$(\rho C)_{nf} = (1 - \chi)(\rho C)_f + \chi(\rho C)_s, \quad (3)$$

$$\sigma_{nf} = \sigma_f \left[1 + \frac{3\left(\frac{\sigma_s}{\sigma_f} - 1\right)\chi}{\frac{\sigma_s}{\sigma_f} + 2 - \left(\frac{\sigma_s}{\sigma_f} - 1\right)\chi} \right]. \quad (4)$$

Phenomenological Laws:

$$\frac{\kappa_{nf}}{\kappa_f} = \frac{\kappa_s + 2\kappa_f - 2\chi(\kappa_f - \kappa_s)}{\kappa_s + 2\kappa_f + 2\chi(\kappa_f - \kappa_s)}, \tag{5}$$

$$\frac{\mu_{nf}}{\mu_f} = (1 - \chi)^{-2.5}. \tag{6}$$

Nanofluid phase [10]:

$$\nabla \cdot U = 0, \tag{7}$$

$$\begin{aligned} \rho_{nf} \left(\frac{\partial U}{\partial t} + \Omega \times U + (U \cdot \nabla)U \right) \\ = \nabla P + \nabla(\mu_{nf} \nabla \cdot U) \\ + F_p + F_b + J \times B, \end{aligned} \tag{8}$$

$$(\rho C)_{nf} \left(\frac{\partial T}{\partial t} + (U \cdot \nabla)T \right) = \nabla(\kappa_{nf} \nabla \cdot T) + Q_p. \tag{9}$$

Dust phase:

$$\nabla \cdot V = 0, \tag{10}$$

$$\rho_p \left(\frac{\partial V}{\partial t} + (V \cdot \nabla)V \right) = -\nabla P - F_p, \tag{11}$$

$$\rho_p C_p \left(\frac{\partial T_p}{\partial t} + (V \cdot \nabla)T_p \right) = -Q_p. \tag{12}$$

The generalized Ohm's law [45]:

$$J + \frac{\omega_e \tau_e}{B_0} \times (J \times B) = \sigma_{nf} \left(E + U \times B + \frac{1}{en_e} P_e \right), \tag{13}$$

here, $U = (u_f, v_f, w_f)$ and $V = (u_p, v_p, w_p)$ are, respectively, the velocity vectors of fluid and dust phase, F_p and F_b are dust particles and body forces, respectively. Equations (7) and (10) are the continuity equations of nanofluid and dust particle flows, respectively. The right-hand side of Eq. (8) is the convective part, whereas $\Omega \times U$ is due to rotational flow. The first term in the left-hand side is due to the pressure gradient; the second one is viscous term. $J \times B$ is because of the applied magnetic field. The right-hand side of Eq. (9) deals with advection, whereas the first term of left-hand side deals with conduction. Thermal interaction between dust particles and nanofluid is Q_p , E the electric field intensity, $B = (0, B_0, 0)$ -magnetic induction. The term F_p is the drag force between the fluid-particles and is defined as

$$F_p = 6\pi N r_p \mu_f (V - U) = \frac{\rho_p (V - U)}{\tau_v}, \tag{14}$$

where the momentum relaxation time of dust phase is $\tau_v = m_p / 6\phi v_f r_p$. The thermal interaction between the particles and the fluid is given by

$$Q_p = \frac{\rho_p C_p (T_p - T)}{\tau_T}, \tag{15}$$

and the thermal relaxation time of the dust phase is $\tau_T = \frac{m_p C_p}{4\phi r_p}$. After ignoring the electric field, the Eq. (13) is

$$J_x = \frac{\sigma_{nf} B_0}{(1 + m^2)} (mu - w), \tag{16}$$

$$J_z = \frac{\sigma_{nf} B_0}{(1 + m^2)} (u + mw), \tag{17}$$

with $m_e = \omega_e \tau_e$ is hall parameter. The governing equations in component forms are [10]:

Nanofluid phase:

See Fig. 1.

$$\frac{\partial u}{\partial x} + \frac{\partial v}{\partial y} = 0, \tag{18}$$

$$\begin{aligned} \left(\frac{\partial u}{\partial t} + u \frac{\partial u}{\partial x} + v \frac{\partial u}{\partial y} \right) = v_{nf} \left(\frac{\partial^2 u}{\partial y^2} \right) + 2\omega w + \frac{\rho_p}{\rho_{nf} \tau_v} (u_p - u) \\ + g \frac{(\rho \beta_T)_{nf}}{\rho_{nf}} (T - T_\infty) - \frac{\sigma_{nf} B_0^2}{\rho_{nf} (1 + m^2)} (u + mw) - \frac{v_{nf}}{K^*} u - Fu^2, \end{aligned} \tag{19}$$

$$\begin{aligned} \left(\frac{\partial w}{\partial t} + u \frac{\partial w}{\partial x} + v \frac{\partial w}{\partial y} \right) = v_{nf} \left(\frac{\partial^2 w}{\partial y^2} \right) - 2\omega u + \frac{\rho_p}{\rho_{nf} \tau_v} (w_p - w) \\ - \frac{\sigma_{nf} B_0^2}{\rho_{nf} (1 + m^2)} (mu - w) - \frac{v_{nf}}{K^*} w - Fw^2, \end{aligned} \tag{20}$$

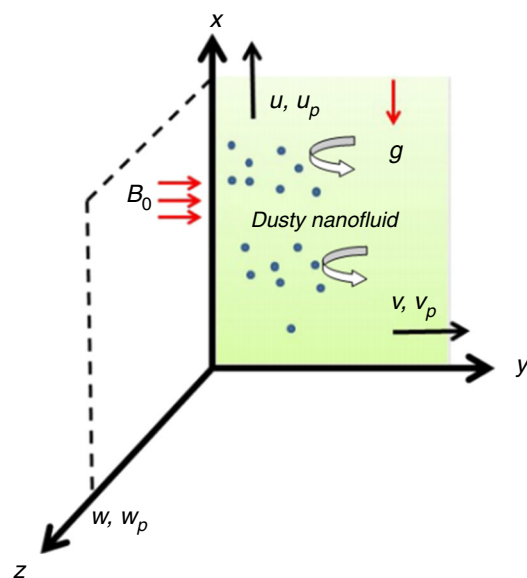


Fig. 1 Geometry of the problem

$$(\rho C)_{\text{nf}} \left(\frac{\partial T}{\partial t} + u \frac{\partial T}{\partial x} + v \frac{\partial T}{\partial y} \right) = \kappa_{\text{nf}} \frac{\partial^2 T}{\partial y^2} + \frac{\rho_p C_p}{\tau_T} (T_p - T) - \frac{\partial q_r}{\partial z}. \quad (21)$$

Dust phase:

$$\frac{\partial u_p}{\partial x} + \frac{\partial v_p}{\partial y} = 0, \quad (22)$$

$$\rho_p \left(\frac{\partial u_p}{\partial t} + u_p \frac{\partial u_p}{\partial x} + v_p \frac{\partial u_p}{\partial y} \right) = \frac{\rho_p}{\tau_v} (u - u_p), \quad (23)$$

$$\rho_p \left(\frac{\partial w_p}{\partial t} + u_p \frac{\partial w_p}{\partial x} + v_p \frac{\partial w_p}{\partial y} \right) = \frac{\rho_p}{\tau_v} (w - w_p), \quad (24)$$

$$\rho_p C_p \left(\frac{\partial T_p}{\partial t} + u_p \frac{\partial T_p}{\partial x} + v_p \frac{\partial T_p}{\partial y} \right) = \frac{\rho_p C_p}{\tau_T} (T - T_p). \quad (25)$$

The corresponding boundary conditions for the governing PDEs are

$$u(x, 0, t) = U_w, v(x, 0, t) = w(x, 0, t) = 0, T(x, 0, t) = T_w, \quad (26)$$

$$\left. \begin{aligned} u(x, y, t) = u_p(x, y, t) = w(x, y, t) = w_p(x, y, t) = 0, \\ u_p(x, y, t) = v(x, y, t), T(x, y, t) = T_p(x, y, t) = T_\infty, \end{aligned} \right\} \text{as } y \rightarrow \infty. \quad (27)$$

We, now, introduce the following dimensionless variables:

$$\left. \begin{aligned} \eta = \sqrt{\frac{b}{v_f(1-\alpha t)}} y, u = \frac{bx}{1-\alpha t} f'(\eta), v \\ = -\sqrt{\frac{bv_f}{(1-\alpha t)}} f(\eta), \theta(\eta) = \frac{T - T_\infty}{T_w - T_\infty}, \\ w = \frac{bx}{1-\alpha t} h(\eta), u_p = \frac{bx}{1-\alpha t} F'(\eta), v_p \\ = -\sqrt{\frac{bv_f}{(1-\alpha t)}} F(\eta), w_p = \frac{bx}{1-\alpha t} H(\eta). \end{aligned} \right\} \quad (28)$$

Both the continuity equations are identically satisfied, while the rest of the equations are transformed as:

$$\begin{aligned} M_2 f''' + M_1 \left(ff'' - f'^2 - S \left(f' + \frac{\eta}{2} f'' \right) \right) + M_4 \lambda \theta + l \beta_v (F' - f') \\ + 2M_1 \Omega h - \frac{M_3 M^2}{1+m^2} (f' + mh) - M_2 \delta f' - M_1 F r f'^2 = 0, \end{aligned} \quad (29)$$

$$\begin{aligned} M_2 h'' + M_1 \left(fh' - f'h - S \left(h + \frac{\eta}{2} h' \right) \right) + l \beta_v (H - h) - 2M_1 \Omega f' \\ + \frac{M_3 M^2}{1+m^2} (mf' - h) - M_2 \delta h - M_1 F r h^2 = 0, \end{aligned} \quad (30)$$

$$\begin{aligned} \left[\frac{\kappa_{\text{nf}}}{\kappa_n} \frac{1}{\text{Pr}} + \frac{4}{3} R d (1 + (\theta w - 1) \theta)^3 \right] \theta'' + M_5 \left[f \theta' - 2f' \theta - S \left(\frac{\eta}{2} \theta' + 2\theta \right) \right] \\ + l \gamma \beta_T (\phi - \theta) + 4R d (\theta w - 1) (1 + (\theta w - 1) \theta)^2 \theta^2 = 0. \end{aligned} \quad (31)$$

Dust phase:

$$F'' F - F'^2 - S \left(F + \frac{\eta}{2} F'' \right) + \beta_v (f' - F') = 0, \quad (32)$$

$$H' F - H F' - S \left(H + \frac{\eta}{2} H' \right) + \beta_v (h - H) = 0, \quad (33)$$

$$\phi' F - 2F' \phi - S \left(\frac{\eta}{2} \phi' + 2\phi \right) + \beta_T (\theta - \phi) = 0. \quad (34)$$

The transformed boundary conditions are:

$$\left. \begin{aligned} f'(0) = 1, f(0) = 0, h(0) = 0, \theta'(0) = \frac{\kappa_n}{\kappa_{\text{nf}}} Bi(1 - \theta(0)), \\ f'(\infty) \rightarrow 0, h(\infty) \rightarrow 0, \theta(\infty) \rightarrow 0, \phi(\infty) \rightarrow 0, \\ F'(\infty) \rightarrow 0, H(\infty) \rightarrow 0, F(\infty) \rightarrow f(\infty). \end{aligned} \right\} \quad (35)$$

where

$$\left. \begin{aligned} M_1 = \left((1 - \kappa) + \kappa \frac{\rho_s}{\rho_f} \right), M_2 = (1 - \kappa)^{-2.5}, \\ M_3 = \left(1 + \frac{3 \left(\frac{\sigma_s}{\sigma_f} - 1 \right) \kappa}{\frac{\sigma_s}{\sigma_f} + 2 - \left(\frac{\sigma_s}{\sigma_f} - 1 \right) \kappa} \right), \\ M_4 = \left((1 - \kappa) + \kappa \frac{(\rho \beta_T)_s}{(\rho \beta_T)_f} \right), M_5 = \left((1 - \kappa) + \kappa \frac{(\rho C)_s}{(\rho C)_f} \right). \end{aligned} \right\} \quad (36)$$

The different dimensionless parameters are defined as

$$\left. \begin{aligned} l = \frac{\rho_p}{\rho_f}, \quad \beta_v = \frac{1 - \alpha t}{\tau_v b}, \quad Gr_x = \frac{g \beta_{Tf}}{b^2 \nu_f^2} (T_w - T_\infty) U_w^2, \\ \beta_T = \frac{1 - \alpha t}{\tau_T b}, \\ Pr = \frac{\mu_p C_p}{\kappa_p}, \quad \gamma = \frac{C_p}{C_f}, \quad M^2 = \frac{\sigma_f B_0^2 (1 - \alpha t)}{\rho_f b}, \quad \lambda = \frac{Gr_x}{Re_x^2}, \\ Re_x = \frac{U_w x}{\nu_f}, \quad S = \frac{\alpha}{b}, \quad \Omega = \frac{\omega}{b} (1 - \alpha t), \\ \delta = \frac{\nu_f}{K^* b} (1 - \alpha t), \\ Fr = \frac{C_b}{K^{*1/2}}, \quad Rd = \frac{4\sigma^*}{\langle \mu C \rangle_f}, \quad \theta_w = \frac{T_w}{T_\infty}, \\ Bi = \frac{h_f}{\kappa_f} \sqrt{\frac{(1 - \alpha t) \nu_f}{b}}. \end{aligned} \right\} \quad (37)$$

The important quantities of interest are the coefficient of skin friction in x and z directions and the local Nusselt number. These are defined as

$$Re_x^{1/2} C_{fx} = \frac{\mu_{nf} \left(\frac{\partial v}{\partial y} \right)_{y=0}}{\rho_f U_w^2} = \frac{1}{(1 - \kappa)^{2.5}} f''(0), \tag{38}$$

$$Re_y^{1/2} C_{fy} = \frac{\mu_{nf} \left(\frac{\partial w}{\partial y} \right)_{y=0}}{\rho_f U_w^2} = \frac{1}{(1 - \kappa)^{2.5}} h'(0), \tag{39}$$

$$Re_x^{-1/2} Nu_x = \frac{-\kappa_{nf} \left(\frac{\partial T}{\partial y} \right)_{y=0}}{\kappa_f (T_w - T_\infty)} = \frac{\kappa_{nf}}{\kappa_f} \theta'(0). \tag{40}$$

Numerical solution and results

The Eqs. (29–34) supporting with boundary conditions (35) are solved numerically by a MATLAB built-in function bvp4c, which is frequently used due to its efficiency and accuracy [46–48]. Recently, Mustafa [49] has discussed the closed analytical solution of two-phase MHD dusty fluid; however, due to nonlinearity, the current problem is addressed numerically. The domain $[0, \infty)$ is replaced with $[0, 5]$, and the results are approximated with the tolerance of 10^{-5} . The higher-order differential equations are transformed to the first-order system of equations along with boundary conditions. The MATLAB function bvp4c is finite difference code that works on three-stage Lobatto IIIa formula. It provides a collocation fourth-order accurate C^1 -continuous solution as this is based on collocation formula. Error control and mesh size based on the residual of the continuous solution. Table 1 shows the calculated results in limiting case using bvp4c code. This table shows the excellent agreement with the results of previously published article. In Table 2, the effect of unsteadiness parameter S , momentum dust parameter β_v , and thermal dust parameter β_t on wall shear stress are presented. It is observed that higher values of unsteadiness parameter S have increasing trend on $f''(0)$, whereas a reverse relation is noticed for $F'(0)$. Both $f''(0)$ and $F'(0)$ increase for the increasing values of momentum and thermal dust parameters; however, this increase is negligible for thermal dust parameter β_t .

Figures 2–15 are plotted to understand the impact of different parameters on velocity and temperature profiles. Figure 2 depicts the influence of momentum dust parameter β_v on the dusty fluid. Figure illustrates that the dust phase moment is enhanced for the higher values of β_v . This

Table 2 Tabular comparison between nanofluid phase and dust phase flow

S	β_v	β_t	$f''(0)$	$F'(0)$
0.10	1.2	1.2	1.215548	0.454667
0.15			1.252207	0.385638
0.20			1.295923	0.289681
0.25			1.352749	0.144532
	1.3		1.218099	0.483579
	1.4		1.220385	0.509462
	1.5		1.222460	0.532789
		1.3	1.215576	0.454667
		1.4	1.215601	0.454668
		1.5	1.215625	0.454668

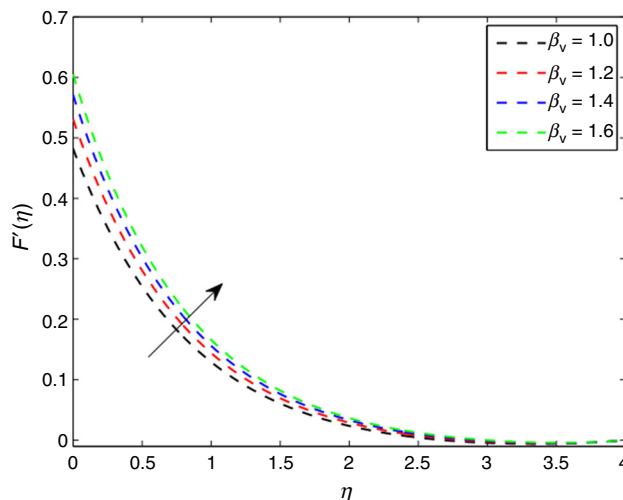


Fig. 2 Influence of β_v on F'

velocity enhances until it matches with the velocity of nanofluid. This increment occurs because of the higher momentum of the dust particles. Both the velocity profiles f' and F' are declined for the larger porosity parameter δ as can be verified in Fig. 3. The existence of porous medium produces a resistance in the flow, and by increasing the porosity parameter means, the size of the pores are enhanced, and hence, a more resistance is produced which decline the velocity as well as the momentum boundary layer thickness. As previously discussed that the velocity

Table 1 Comparison of $-\theta'(0)$ values for different values of Pr when the rotational effects, Darcy Forchimer flow and nonlinear thermal radiations are ignored

Pr	Chen (FDM)	Abel et al. (RK method)	Gireesha et al. (RKF-45)	Present (bvp4c)
0.72	1.0885	1.0885	1.0885	1.08854
1.0	1.3333	1.3333	1.3333	1.33333
3.0	2.5097	–	2.5097	2.50971
10.0	4.7968	4.7968	4.7968	4.79682

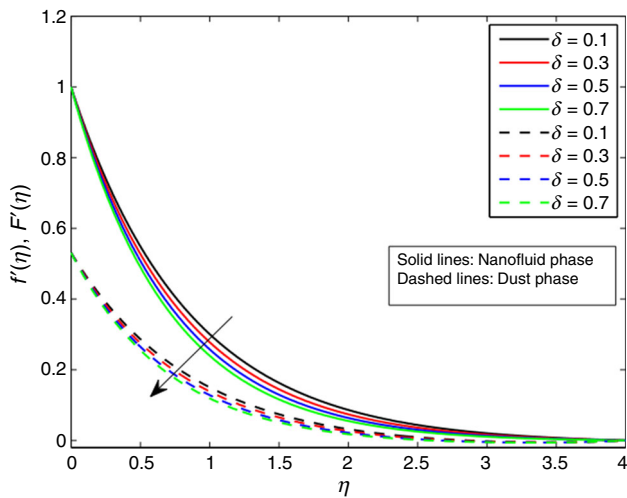


Fig. 3 Influence of δ on f' and F'

decreases because of the porous medium, however, this decrement is more prominent after the inclusion of inertial effects Fr , and this phenomenon is presented in Fig. 4. The impact of mass concentration of dust particles l on velocity profiles for the dusty and nanofluid flow is shown in Fig. 5. It is observed that by adding the more dust particles, the drag force is enhanced which reduces the speed of the fluid. The Lorentz forces are generated more hastily when the applied magnetic field is enhanced. As these are the opposing forces in nature, so the velocities f' and F' are lessens as shown in Fig. 6. Figure 7 illustrates how the increasing rotational parameter effects the velocities profiles. It is noticed that both the velocities of dusty fluid F' and nanofluid f' are diminished along with hydrodynamic boundary layer thickness due to higher rotation in fluid when compared with the stretching rate. Effects on temperature profiles for the different parameters are portrayed in Figs. 8–10. Figure 8 predicts the Prandtl number effects

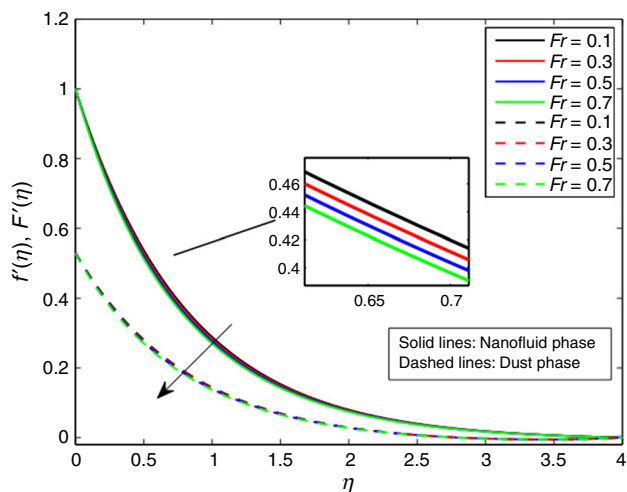


Fig. 4 Influence of Fr on f' and F'

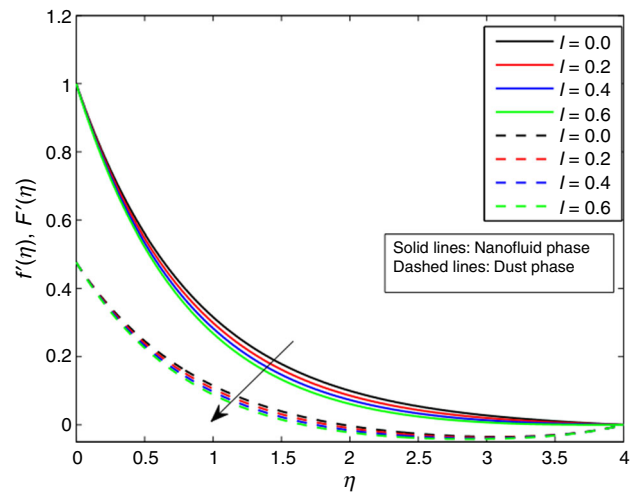


Fig. 5 Influence of l on f' and F'

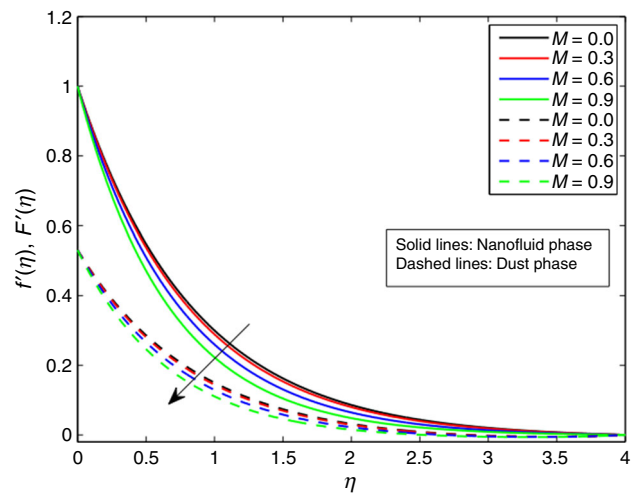


Fig. 6 Influence of M on f' and F'

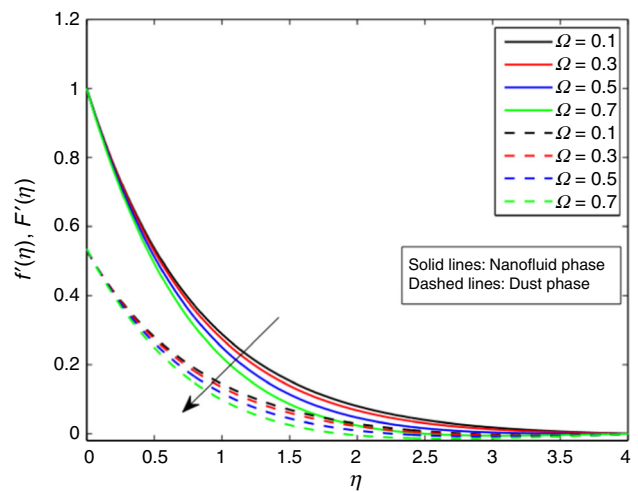


Fig. 7 Influence of Ω on f' and F'

on the temperature profiles for nanofluid and dusty fluid flows. Prandtl number is the ratio of momentum diffusivity to thermal diffusivity. Thermal diffusivity is reduced when Pr is increased. Due to this decrement in thermal diffusion, the thermal boundary layer got thinner, and hence, the temperature of the fluid decreases. The temperature of the fluid $\theta(\eta)$ and $\phi(\eta)$ is rapidly enhanced when the thermal radiation parameter is taken larger as stated in Fig. 9. Due to the radiation, the heat is transferred into the fluid which augments the thermal boundary layer of nanofluid and dusty fluid. Figure 10 shows the variation of temperature ratio parameter θ_w in the temperature profile of nanofluid and dusty fluid, respectively. θ_w is the ratio between the wall temperature and ambient temperature. As wall temperature escalates when temperature ratio parameter is increased, the temperature rises. In Fig. 11, the characteristics of Hall current parameter m on transverse velocity components $h(\eta)$ and $H(\eta)$ are considered. Both the velocities are upgraded significantly when the value of m is uprooted. It happens because of the reason that the larger values of m decrease the conductivity of $\frac{\sigma_f}{1+m^2}$, and magnetic damping force rises up. Through Fig. 12, it is observed that the tangential velocities of nanofluid phase $h(\eta)$ and dust phase $H(\eta)$ both are increased near the surface $\eta < 1$, but gradually, they decreases away $\eta > 1$ from the wall when the magnetic field is increased. The skin friction coefficient along the x -axis for the magnetic parameter M , unsteadiness parameter S , Hall current parameter m and momentum dust phase parameter β_v is highlighted in Figs. 13 and 14. These figures shows that the Hall current parameter enhances the skin friction where as the increasing values of magnetic parameter, unsteadiness parameter and momentum for the dust particles parameter

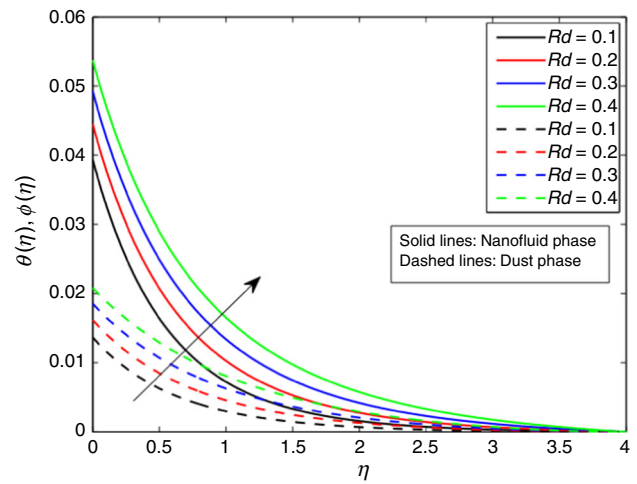


Fig. 9 Influence of Rd on θ and ϕ

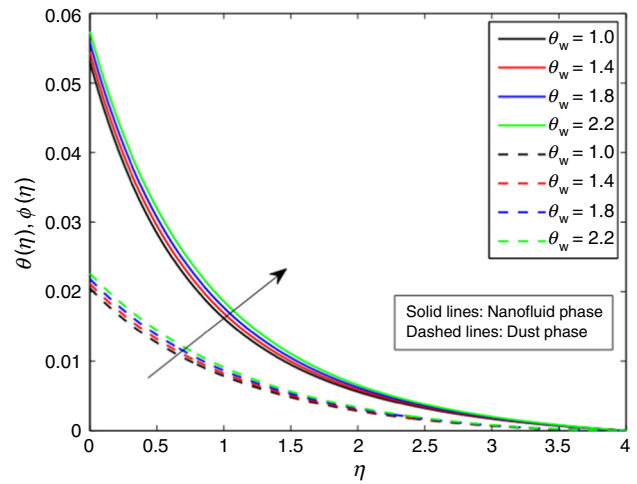


Fig. 10 Influence of θ_w on θ and ϕ

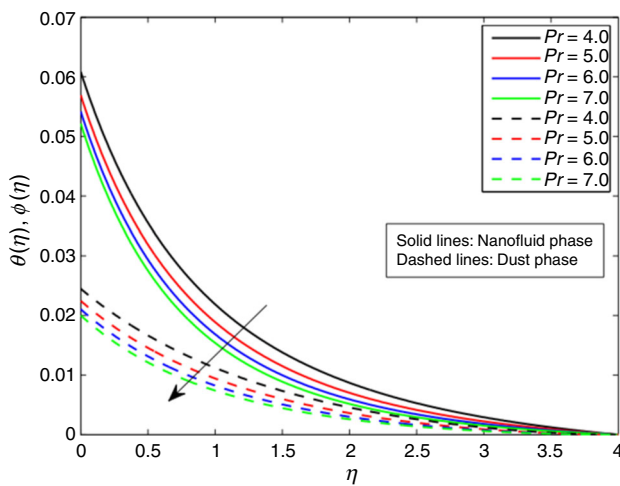


Fig. 8 Influence of Pr on θ and ϕ

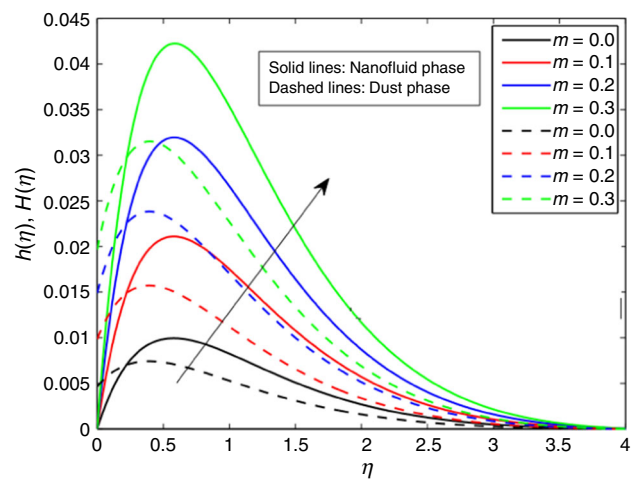


Fig. 11 Influence of m on $h(\eta)$ and $H(\eta)$

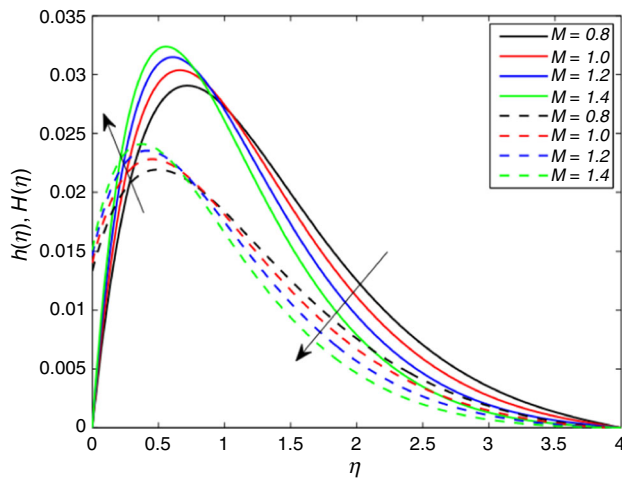


Fig. 12 Influence of M on $h(\eta)$ and $H(\eta)$

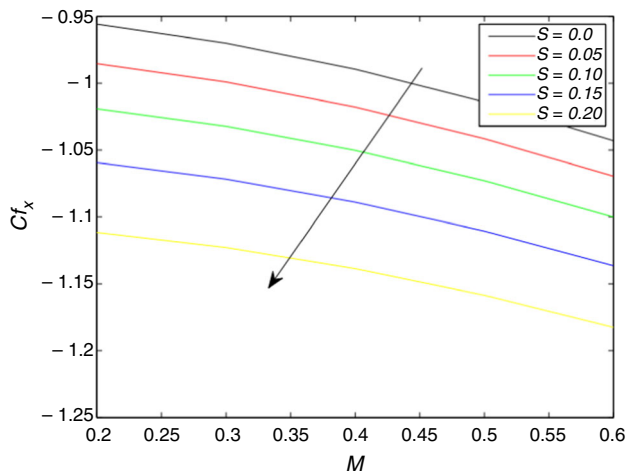


Fig. 13 Influence of S and M on $Cf_x Re_x^{1/2}$

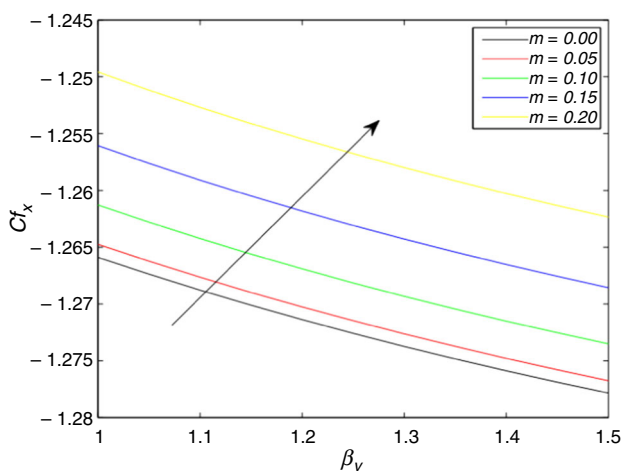


Fig. 14 Influence of m and β_v on $Cf_x Re_x^{1/2}$

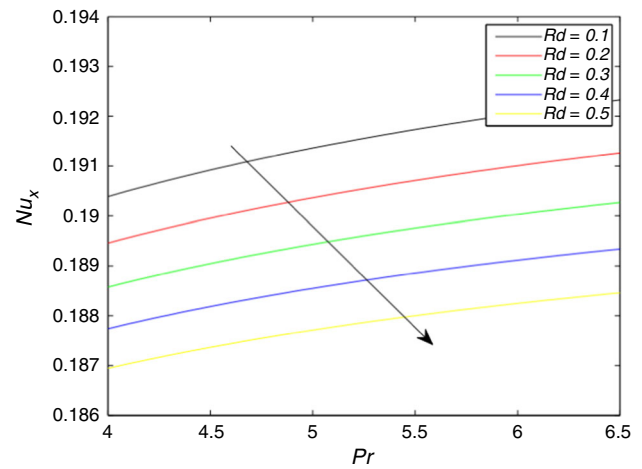


Fig. 15 Influence of Rd and Pr on $Nu_x Re_x^{-1/2}$

are responsible for the reduction of drag force on the surface. Figure 15 shows the rate of heat transfer on the wall for different parameters such as thermal radiation parameter Rd and Prandtl number Pr . The dimensionless Nusselt number escalates for the higher values of Prandtl number; however, a reverse relation is noticed for the thermal radiation parameters i.e., Rd .

Concluding remarks

This article comprises the numerical discussion of unsteady MHD dusty nanofluid rotating flow over the convected surface with nonlinear thermal radiation and non-Darcian effects. Carbon nanotubes are considered as the nanoparticles, and Hall current phenomenon is produced due to the higher magnetic strength. A MATLAB function `bvp4c` is utilized to solve the equations. The main findings are as listed below.

- Due to the increment of inertial coefficient, the velocity of the dust phase and nanofluid phase both decreases..
- Rotational coefficient and velocity profiles are reciprocal of each other.
- The thermal and flow field of nanofluid are much more higher than the dust phase.
- Thermal boundary layer of nanofluid and dust phase fluids are raised for the higher values of radiation parameter.
- Temperature and velocity boundary layer are enhanced in the presence of dust particles.
- Thermal field is declined, while velocities are inclined for the Hall current effect.
- The Nusselt number is reduced when the temperature ratio is increased

References

- Doronin GG, Larkin NA. Mathematical problems for a dusty gas flow. *Boletim Da Sociedade Paranaense de Matematica Terceira Serie*. 2004;22(1):21–9.
- Farbar L, Morley MJ. Heat transfer to flowing gas-solid mixtures in a circular tube. *Ind Eng Chem*. 1957;49:1143–50.
- Saffman PG. On the stability of laminar flow of a dusty gas. *J Fluid Mech*. 1962;13:120–8.
- Attia HA, Abbas W, Abdeen MAM. Ion slip effect on unsteady Couette flow of a dusty fluid in the presence of uniform suction and injection with heat transfer. *J Braz Soc Mech Sci Eng*. 2016;38(8):2381–91.
- Koneri LK, Gireesha BJ, Mahanthesh B, Gorla RSR. Influence of nonlinear thermal radiation and magnetic field on upper-convected Maxwell fluid flow due to a convectively heated stretching sheet in the presence of dust particles. *Commun Numer anal*. 2016;1:57–73.
- Sandeep N, Sulochana C, Kumar BR. Unsteady MHD radiative flow and heat transfer of a dusty nanofluid over an exponentially stretching surface. *Eng Sci Technol Int J*. 2016;19:227–40.
- Pop I, Hamid RA, Nazar R. Boundary layer flow of a dusty fluid over a permeable shrinking surface. *Int J Numer Methods Heat Fluid Flow*. 2017;27(4):1–19.
- Ghadikolaei SS, Hosseinzadeh K, Yassari M, Sadeghi H, Ganji DD. Boundary layer analysis of micropolar dusty fluid with TiO_2 nanoparticles in a porous medium under the effect of magnetic field and thermal radiation over a stretching sheet. *J Mol Liq*. 2017;244:374–89.
- Siddiqua S, Begum N, Ouazzi A, Hossain MA, Gorla RSR. Heat transfer analysis of Casson dusty fluid flow along a vertical wavy cone with radiating surface. *Int J Heat Mass Transf*. 2018;127:589–96.
- Gireesha BJ, Mahanthesh B, Thammanna GT, Sampathkumar PB. Hall effects on dusty nanofluid two-phase transient flow past a stretching sheet using KVL model. *J Mol Liq*. 2018;256:139–47.
- Bear J. *Dynamics of fluids in porous media*. New York: Dover; 1972.
- Hellstrom JGI, Lundstrom TS. Flow through porous media at moderate Reynolds number. In: 4th Int. Sci. Colloquium: Model. Mat. Proc. Uni. Latvia, Riga, Latvia; 2006. p. 8–9.
- Sobieski W, Trykozko A. Darcy's and Forchheimer's laws in practice. Part 1. The experiment. *Tech. Sci*. 2014;17(4):321–35.
- Chapman RE. *Geology and water: an introduction to fluid mechanics for geologists*. The Hague: Martinus Nijho & Dr. W. Junk Publishers; 1981.
- Forchheimer P. *Wasserbewegung durch boden*. Z. Ver D. Ing. 1901;45:1782–8.
- Ewing R, Lazarov R, Lyonss L, Papavassiliou DV, Pasciak J, Qin GX. Numerical well model for non-Darcy flow. *Comput. Geosci*. 1999;3(3):185–204.
- Shehzad SA, Abbasi FM, Hayat T, Alsaedi A. Cattaneo-Christov heat flux model for Darcy-Forchheimer flow of an Oldroyd-B fluid with variable conductivity and non-linear convection. *J Mol Liq*. 2016;224:274–8.
- Rami YJ, Fawzi A, Fahmi AAR. Darcy-Forchheimer mixed convection heat and mass transfer in fluid saturated porous media. *Int J Numer Methods Heat Fluid Flow*. 2001;11(6):600–18.
- Sobieski W, Trykozko A. Sensitivity aspects of Forchheimers approximation. *Trans Porous Media*. 2011;89(2):155–64.
- Hayat T, Haider F, Muhammad T, Alsaedi A. Darcy-Forchheimer flow with Cattaneo-Christov heat flux and homogeneous heterogeneous reactions. *PLoS ONE*. 2017;12(4):e0174938.
- Muhammad T, Alsaedi A, Shehzad SA, Hayat T. A revised model for Darcy Forchheimer flow of Maxwell nanofluid subject to convective boundary condition. *Chin J Phys*. 2017;55(3):963–76.
- Sajid T, Sagheer M, Hussain S, Bilal M. Darcy-Forchheimer flow of Maxwell nanofluid flow with nonlinear thermal radiation and activation energy. *AIP Adv*. 2018;8:035102.
- Alzahrani AK. Importance of Darcy Forchheimer porous medium in 3D convective flow of carbon nanotubes. *Phys Lett A*. 2018;382(42):2938–43.
- Majeed A, Zeeshan A, Alamri SZ, Ellahi R. Heat transfer analysis in ferromagnetic viscoelastic fluid flow over a stretching sheet with suction. *Neural Comput Appl*. 2018;30(6):1947–55.
- Alamri SZ, Ellahi R, Shehzad N, Zeeshan A. Convective radiative plane Poiseuille flow of nanofluid through porous medium with slip: an application of Stefan blowing. *J Mol Liq*. 2018;273:292–304.
- Shehzad N, Zeeshan A, Ellahi R, Rashidi S. Modelling study on internal energy loss due to entropy generation for non-Darcy poiseuille flow of silver-water nanofluid: an application of purification. *Entropy*. 2018;20:851.
- Hassan M, Marimb M, Alsharif A, Ellahi R. Convective heat transfer flow of nanofluid in a porous medium over wavy surface. *Phys Lett A*. 2018;382(38):2749–53.
- Hassan M, Marimb M, Alsharif A, Ellahi R. Numerical investigation and optimization of mixed convection in ventilated square cavity filled with nanofluid of different Inlet and outlet port. *Int J Numer Methods Heat Fluid Flow*. 2017;27(9):2053–69.
- Rashidi S, Akar S, Bovand M, Ellahi R. Volume of fluid model to simulate the nanofluid flow and entropy generation in a single slope solar still. *Renew Energy*. 2018;115:400–10.
- Khanafar K, Vafai K. Applications of nanofluids in porous medium. *J Therm Anal Calorim*. 2019;135:1479–92.
- Freidounimehr N, Rahimi AB. Brownian motion effect on heat transfer of a three-dimensional nanofluid flow over a stretched sheet with velocity slip. *J Therm Anal Calorim*. 2019;135:207–22.
- Ramzan M, Bilal M, Chung JD. Radiative Williamson nanofluid flow over a convectively heated Riga plate with chemical reaction—a numerical approach. *Chin J Phys*. 2017;55:1663–73.
- Ramzan M, Bilal M, Chung JD. Effects of thermal and solutal stratification on Jeffrey magneto-nanofluid along an inclined stretching cylinder with thermal radiation and heat generation/absorption. *Int J Mech Sci*. 2017;131:317–24.
- Turkyilmazoglu M. Buongiorno model in a nanofluid filled a symmetric channel fulfilling zero net particle flux at the walls. *Int J Heat Mass Transf*. 2018;126:974–9.
- Turkyilmazoglu M. Fluid flow and heat transfer over a rotating and vertically moving disk. *Phys Fluids*. 2018;30:063605.
- Zeeshan A, Ijaz N, Abbas T, Ellahi R. The sustainable characteristic of Bio-Bi-phase flow of peristaltic transport of MHD Jeffrey fluid in the human body. *Sustainability*. 2018;10:2671.
- Turkyilmazoglu M. Equivalences and correspondences between the deforming body induced flow and heat in two-three dimensions. *Phys Fluids*. 2016;28:043102.
- Turkyilmazoglu M. Analytical solutions to mixed convection MHD fluid flow induced by a nonlinearly deforming permeable surface. *Commun Nonlinear Sci Numer Simul*. 2018;63:373–9.
- Timofeeva VE, Roubort JL, Signh D. Particle shape effects on thermophysical properties of alumina nanofluids. *J Appl Phys*. 2009;106(1):014304.
- Murshed SMS, Nietode Castro CA, Lourenco MJV, Lopes MLM, Santos FJV. A review of boiling and convective heat transfer with nanofluids. *Renew Sustain Energy Rev*. 2011;15(5):2342–54.
- Hussien AA, Yusop NM, Abdullah MZ, Al-Nimr MA, Khavarian M. Study on convective heat transfer and pressure drop of MWCNTs water nanofluid in mini-tube. *J Therm Anal Calorim*. 2019;135:123–32.

42. Padilha GS, Campos VAB, Costa MC, Franco TT. Multi-walled carbon nanotubes used as support for lipase from *Burkholderia cepacia*. *J Therm Anal Calorim*. 2018;134(2):1021–9.
43. Choi SUS, Zang ZG, Yu Z, Lookwood FE, Grulke EA. Anomalous thermal conductivity enhancement in nanotube suspensions. *Appl Nanosci Appl Phys Lett*. 2001;79:2252–4.
44. Kandasamy R, Mohammad R, Muhaimin I. Carbon nanotubes on unsteady MHD non-Darcy flow over porous wedge in presence of thermal radiation energy. *Appl Math Mech Engl*. 2016;37(8):1031–40.
45. Bilal M, Hussain S, Sagheer M. Boundary layer flow of magneto-micropolar nanofluid flow with Hall and ion-slip effects using variable thermal diffusivity. *Bull Pol Acad Tech Sci*. 2017;65(3):383–90.
46. Ramzan M, Bilal M, Chung JD. Soret and Dufour effects on three dimensional upper-convected Maxwell fluid with chemical reaction and non-linear radiative heat flux. *Int J Chem Reactor Eng*. 2017;15(3):20160136.
47. Lu DC, Ramzan M, Bilal M, Chung JD, Farooq U. A numerical investigation of 3-D MHD rotating flow with binary chemical reaction, activation energy and non-Fourier heat flux. *Commun Theor Phys*. 2018;70:89–96.
48. Hayat T, Muhammad T, Shehzad SA, Alsaedi A. On magneto-hydrodynamic flow of nanofluid due to a rotating disk with slip effect: a numerical study. *Comput Methods Appl Mech Eng*. 2017;315:467–77.
49. Turkyilmazoglu M. Magnetohydrodynamics two-phase dusty fluid flow and heat model over deforming isothermal surfaces. *Phys Fluids*. 2017;29:013302.

Publisher's Note Springer Nature remains neutral with regard to jurisdictional claims in published maps and institutional affiliations.